coatings

MDPI

Article

On the Icephobic Behavior of Organosilicon-Based Surface Structures Developed Through Atmospheric Pressure Plasma Deposition in Nitrogen Plasma

Siavash Asadollahi [1,2], Masoud Farzaneh [1] and Luc Stafford [2,*]

[1] Canada Research Chair on Engineering of Power Network Atmospheric Icing (INGIVRE), Université du Québec à Chicoutimi, Saguenay, QC G7H 2B1, Canada; siavash.asadollahi@umontreal.ca (S.A.); Masoud_Farzaneh@uqac.ca (M.F.)

[2] Département de Physique, Université de Montréal, Montréal, QC H3T 1J4, Canada

* Correspondence: luc.stafford@umontreal.ca; Tel.: +1-514-343-6542

Received: 19 September 2019; Accepted: 17 October 2019; Published: 18 October 2019

Abstract: In many regions around the world, atmospheric icing during freezing rains and ice storms can cause severe damage to exposed infrastructure. Subsequently, protective coatings capable of ice accumulation prevention or ice adhesion reduction, often referred to as icephobic coatings, have gained a significant amount of interest. In this study, we examine an atmospheric-pressure plasma jet technique for the development of organosilicon-based icephobic coatings on aluminum substrates. Initially, Al-6061 samples are exposed to multiple passes of air plasma treatment at very short jet-to-substrate distances to create a microporous alumina-based surface structure. These surfaces are then used for plasma deposition of superhydrophobic coatings in the same jet with hexamethyldisiloxane (HMDSO) as the precursor and nitrogen as the plasma gas. Several samples are created with varying plasma precursor flow rates and number of deposition passes. All samples are exposed to three cycles of icing/de-icing to estimate coatings' stability in aggressive natural conditions. The effects of multiple icing/de-icing cycles on surface chemistry, surface morphology, and wetting behavior is studied. It is shown that the most remarkable mechanism through which icing affects surface properties is coating removal during aggressive de-icing procedure. Finally, the icephobic properties of the most efficient coating (referred to as PT5x3) is further studied through 10 cycles of icing/de-icing, and it is shown that this coating can reduce ice adhesion strength by a factor of at least two for up to nine cycles of icing/de-icing.

Keywords: atmospheric pressure plasma jet; organosilicon-based coatings; atmospheric icing; icephobicity; superhydrophobicity; wetting

1. Introduction

Several countries around the world such as Canada, United States of America, Sweden, Norway, Russia, and China contend with ice-related problems on a yearly basis. Ice accumulation during different atmospheric events, if not addressed swiftly and with precision, can lead to power shortages, driving and aviation accidents as well as significant life hazards. Glaze ice, which is formed by the instantaneous solidification of super-cooled water droplets upon impact with exposed structures, is the most problematic form of atmospheric icing due to its density, hardness, and adhesion to the surface. Specifically, for power transmission networks, formation of glaze ice can lead to catastrophic failure [1]. To prevent failure, power companies have attempted to build overhead lines and transmission towers that are capable of withstanding large icing events. This requires strengthened towers and expensive lines, which will increase the construction and maintenance cost [2,3]. To avoid such excessive costs

while preventing the failure of power transmission networks under icing conditions, a solution should be found to either remove the ice from the surface through mechanical or thermal means (active icing protection) or prevent its accretion through a protective coating on the surface (passive icing protection). The term "icephobic coating" is broadly used to refer to such coatings, but no conclusive definition for icephobicity exists in the literature. Some studies define icephobicity as low adhesion strength between ice and a solid surface [4–8]. In this case, ice adhesion strength can refer to shear stress [9,10] or normal stress [11–13]. Some other studies define icephobicity as the ability to prevent, delay, or reduce ice accumulation [13,14]. However, the data presented in such studies is greatly dependent on the methodology used for ice accumulation and ice removal: several factors, such as thermal expansion of ice, stress distribution and loading rate during ice removal, environmental conditions during and after ice accretion, or salinity of water used for ice accumulation may affect the ice adhesion data. This introduces a great deal of difficulty in comparing different icephobic coatings introduced in the literature [9]. The quantitative values ranging from tens of kPa [15] to 1 MPa [16] are reported, but a majority of values are in the range of hundreds of kPa [17,18]. In some cases, the adhesion strength value determined for the same sample can vary by multiples orders of magnitude when a different de-icing method is used [16]. To address these inconsistencies, some studies report on the adhesion reduction factor (ARF), which is defined as the ratio between ice adhesion strength on a given icephobic surface to the ice adhesion strength on an untreated (control) sample [19].

Conventionally, the development of icephobic surfaces is closely related to superhydrophobicity. Generally, wetting characteristics is studied to better evaluate the icing properties of a surface. Several studies suggest that superhydrophobic surfaces can exhibit icephobic behavior [2,20–26]. While hydrophobic coatings are shown to be able to reduce the ice adhesion strength to some extent, it has been unclear how this reduction correlates with various measurements of a superhydrophobic surface. This uncertainty was changed when a strong linear correlation was reported between ice adhesion strength and a water wetting related parameter [6,27]:

$$\tau \propto [1 + \cos \theta_{rec}] \quad (1)$$

where τ is the ice adhesion strength and θ_{rec} is the receding angle for a water droplet. $[1 + \cos \theta_{rec}]$ scales with the practical work of adhesion, which is the energy required to remove a water droplet from a surface [28]. Meuler et al. studied the ice adhesion strength data from three separate studies (Meuler et al. [6], Dotan et al. [29], and Kulinich and Farzaneh [4]) performed on different sets of surfaces and found a linear relationship between ice adhesion strength and $[1 + \cos \theta_{rec}]$, regardless of the ice deposition process and measurement method used [30]. This correlation is further discussed in Section 3.1.

Several studies have cast doubts on the correlation between superhydrophobicity and icephobicity [31–33]. It is often argued that it is not accurate to expect any given superhydrophobic surface to be icephobic. For instance, if the surface features are large enough for water droplets penetration (Wenzel wetting regime), ice adhesion may be increased with contact angle. However, some other studies reveal a correlation between superhydrophobicity and icephobicity [13,22,34–39]. It has been shown that a low contact angle hysteresis is a defining criterion in icephobicity [4,19,40,41]. Surfaces with low contact angle hysteresis showed lower ice adhesion strength along with longer delays in freezing times. This suggests that icephobicity is more likely to be achieved in Cassie–Baxter wetting regime. In fact, Meuler et al. have suggested that effective icephobic surfaces must resist transition to fully wetted Wenzel regime that may be brought about by the kinetic energy of impinging water droplets or by the condensation moisture from the ambient atmosphere within the micro and/or nanotextures of the substrates [30]. In Cassie ice, the contact area between ice and substrate is significantly reduced, resulting in a reduction of ice adhesion strength, whereas in Wenzel ice, the real contact area is increased due to surface morphology, leading to an increase in total ice adhesion [42].

Recently, a few studies further investigated the correlation between hydrophobicity and icephobicity [43] and suggested that a superhydrophobic surface can reduce or prevent the ice accretion by one or more of the following mechanisms:

- The heat transfer between the droplet and the surface is hindered by the insulation effect of the nano-structured roughness on the surface. In other words, the micro/nano structure on a superhydrophobic surface acts as an insulating layer on the interface to reduce the heat flux between the liquid and the substrate [22,35,38].
- In a superhydrophobic surface, contact area between the surface and the water droplet is significantly smaller and therefore, less potential nucleation points are available on the surface. Lower contact area results in higher activation energy for nucleation and growth of the ice crystals. It has been shown that for a superhydrophobic surface, the contributions of solid/liquid interface to the solidification process are negligible [22]. In this case, homogeneous nucleation (which is known to have significantly higher activation energies), is dominant. Moreover, smaller contact area can lead to lower heat transfer between the droplet and the surface, which subsequently delays the freezing point [13].
- Unlike hydrophilic surfaces, water droplets are extremely mobile on a superhydrophobic surface and will rebound upon impact. The time for which the water droplet is in contact with the surface before rebounding on a superhydrophobic surface is referred to as the droplet rebound time or shedding time. Mishchenko et al. used high speed imaging to study the impact mechanism and rebound time on several morphologies [44]. They showed that the droplet rebound time can be as short as 20 ms in some cases. If the drop rebound time is smaller than the time needed for ice nucleation, then it can be expected that the ice formation is reduced or prevented [34,37,44–47].

Although the correlation between superhydrophobicity and icephobicity is often expressed in the literature, several case-dependent factors exist that can increase the ice adhesion strength and thus weaken the icephobic characteristics on a superhydrophobic surface. Unfortunately, most of the studies done in this regard only report the superhydrophobicity and/or icephobicity of the surface, and only a few studies have been done on the stability of such surfaces under various conditions such as UV exposure or multiple consecutive icing/de-icing cycles. Even when some sort of durability investigation is performed for an icephobic sample, the data is strongly dependent on the icing and/or de-icing method used. For instance, Boinovich et al. [48] have presented contact angle data after 100 icing de-icing cycles. However, the icing procedure in their work consists of placing the samples in contact with distilled water at low temperature, while de-icing procedure is simply increasing the temperature until the ice thaws on the surface. In another example of hundred of icing/deicing cycles [49], ice is formed on the surface by simply placing a water droplet on the substrate and reducing the temperature until the droplet is frozen. The ice is then removed by straining the substrate. Compared to methods where ice shedding is done through applying shear or normal stress to the accumulated ice, these deicing methods are significantly less aggressive towards the coating, and thus coatings that can maintain some sort of icephobic properties after hundreds of "cycles" are not unusual. In fact, to the best of our knowledge, when an aggressive de-icing method is chosen to remove the ice from the surface by applying (controlled) shear or normal stress to the ice layer, icing cycles are usually limited to 10–20 cycles [4–6]. It should be noted that the number of icing/deicing cycles in such cases cannot be correlated to the number of icing events in natural conditions. In any case, for practical applications, the surface should sustain different natural environments, from severe sub-zero conditions and freezing rains in winter to extreme UV exposure and hot weather in summer. It is well known that most of the current coatings will degrade after exposure to several icing/de-icing cycles [5,16,22,48]. Ice build-up and subsequent shedding can destroy the micro/nano-structured roughness on the surface as well as altering the chemical composition of the coating. Therefore, assuming the wide application of such surfaces in outdoor environments, the icephobic characteristics will diminish over time. Another issue which must be addressed is the effect of humidity on the performance of icephobic coatings. Water

condensation in humid conditions can degrade the hydrophobic behavior of a surface by covering the roughness features with water and increase the liquid-solid contact area. Similarly, it was shown that in icephobic applications, frost formation in a supersaturated environment prior to freezing is of significant importance [5,8,48,49]. Before the water solidification, frost can cover the micro/nano structure on the surface, thus reducing the hydrophobicity of a surface and increasing the ice adhesion strength. In this case, ice adhesion strength was shown to increase linearly with surface area, suggesting that frost can cover the whole structure, including post tops, side walls, and valleys [8]. However, it has been suggested that hierarchical structures (surface with multiple levels of roughness) can significantly reduce frost formation. For instance, the wings of Morpho Nestira, a butterfly species native to south and Central America, retain its superhydrophobic properties even in low temperatures and high humidity due to the micro/nano-structured hierarchical surface structure [50], while the superhydrophobic properties of lotus leaf (with only one level of roughness in the range of nanometers) deteriorates rapidly as the temperature decreases or as the humidity increases. This was shown to depend on the area fraction of the solid surface in contact with the liquid (f_1) [51]. A threshold of $f_1 < 0.068$ for the frost-formation prevention was also defined, which suggests a relationship between frost formation and water wetting regime, since a smaller f_1 value corresponds to wetting regimes closer to Cassie–Baxter [52].

Hexamethyldisiloxane, or HMDSO, is an organosilicon precursor well-known and widely used in low pressure and atmospheric pressure plasma treatment applications due to several environmental, economical, and technical factors [53–57]. It consists of a siloxane group (Si–O–Si) bonded to six methyl ($–CH_3$) groups. Since methyl is a low surface energy component [58], HMDSO is also considered to be a prime candidate for hydrophobic and superhydrophobic applications. Numerous studies have reported the development of hydrophobic coatings using HMDSO through various methods and geometries: Superhydrophobic/icephobic coatings were also developed on the surface of anodized aluminum samples though low pressure plasma polymerization with HMDSO as the precursor [59]. These coatings were shown to be relatively stable against natural factors and could maintain their icephobic behavior after 15 cycles of icing/deicing. However, low pressure plasma treatment requires expensive vacuum chambers and pumping system, which can be very expensive, complicated, and impractical for large samples. Atmospheric pressure treatment on the other hand, can be much cheaper with higher growth rates compared to equivalent low-pressure systems, and may be easily implemented in production lines in a wide range of industries. For instance, the deposition time in low-pressure for the HMDSO-based icephobic coating mentioned above is 25 min, which is significantly longer than that of similar coatings in atmospheric pressure (between 1 and 3 min) [60]. Furthermore, coatings deposited under low pressure plasma polymerization are significantly thinner (few nanometers thickness in low-pressure compared to several micrometers in the case of atmospheric deposition) with a drastically different surface morphology.

In this study, a passive icing protection method based on treatment of Al-6061 by atmospheric-pressure plasma jet is examined and the efficiency of such method is studied. Pre-treated aluminum samples are used as substrate for coating deposition in nitrogen plasma with hexamethyldisiloxane (HMDSO) as the precursor. The effects of some of the jet parameters on surface morphology, surface chemistry, wetting behavior, and icephobic characteristics is studied. Finally, the effects of some of the most common environmental factors on surface efficiency for icephobic applications are investigated.

2. Experimental Procedure

First, $30 \times 50 \times 1.8$ mm^3 samples were cut from Al-6061 sheets provided by ALCAN. For all plasma treatment procedures, a commercial OpenAir AS400 atmospheric pressure plasma jet (APPJ) manufactured by PlasmaTreat® (Elgin, IL, USA) with a PFW10 nozzle was used. The schematics of the jet is presented in Figure 1a. The process was open to ambient air and was carried out at room temperature and in uncontrolled humidity conditions. At first, the samples were exposed to multiple scans of air plasma treatment at very short jet-to-substrate distances to generate an alumina-based

micro-roughened porous surface structure on the aluminum substrate (Figure 2). The details of this process, which is driven by the formation of electric discharges between the rotating arc inside the jet body and the substrate, were previously studied by the authors [61]. These "pre-treated" samples were then cleaned in an ultrasonic bath of ethanol and de-ionized water (15 min each at room temperature) to remove any surface contamination prior to coating deposition. For deposition step, the plasma jet was slightly modified with a quartz tube (Figure 1b) mounted on the jet-head. The effects of this modification on surface morphology, surface chemistry, and Si–O network structural integrity is discussed elsewhere [60]. HMDSO (Sigma-Aldrich®, St. Louis, MO, USA, >98%) was used as the growth precursor. Nominally pure nitrogen gas was purchased from Praxair and was used as received. All samples studied here were prepared by the injection of HMDSO vapor (vaporized at 125 °C) mixed with a carrier gas (nitrogen) into the flowing afterglow region of a nitrogen plasma on pre-treated aluminum surfaces.

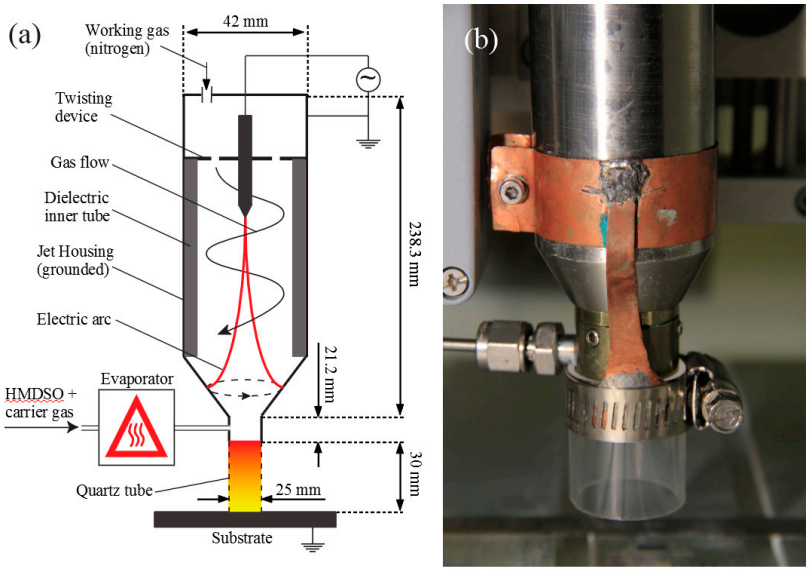

Figure 1. (**a**) Schematics of the modified atmospheric pressure plasma jet (APPJ) used in this study and (**b**) a closer look at the modified plasma jet.

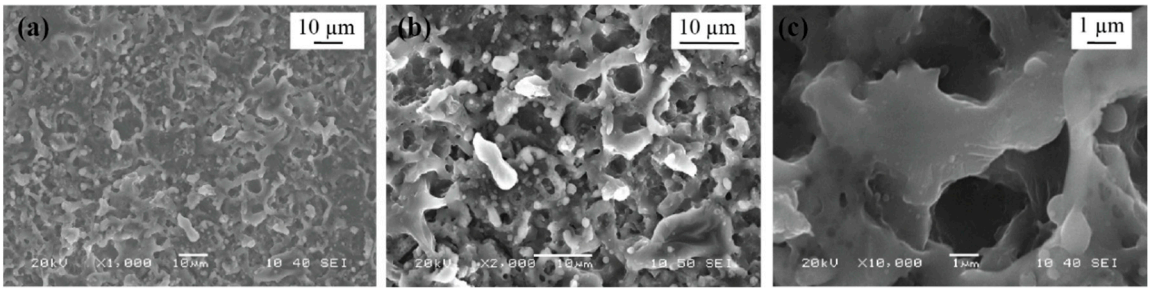

Figure 2. Micro-structure formed on the surface after three passes of air plasma treatment. Samples are coated with conductive carbon prior to image acquisition. The results are shown for different magnifications: (**a**) ×1000, (**b**) ×2000, and (**c**) for 10,000.

Deposition parameters were chosen in a way to highlight the effects of plasma parameters on surface properties. In total, five samples were prepared (Table 1). For all samples, plasma power was set to 500 W, plasma duty cycle (t_{on}/t_{cycle}) to 50%, jet speed to 1 m/min, jet-substrate distance to 30 mm, ionization gas flow rate to 400 L/h, and carrier gas flow rate to 400 L/h. To study the effects of precursor flow rate on the icing behavior of the coatings, PT3 and PT5 were created with a precursor flow rate of 3 and 5 g/h, respectively. Furthermore, to study the effects of multiple deposition passes on icephobic behavior, PT3x3 was created with three deposition passes with identical plasma conditions to PT3 with

three deposition passes, and PT5x3 and PT5x6 were created with identical plasma conditions to PT5 with three and six deposition passes, respectively. The rest of the plasma parameters, summarized in Table 1, were identical for all cases.

Table 1. Plasma conditions used for preparation of samples.

Sample Name	Monomer Flow Rate	Plasma Power	Plasma Duty Cycle	Jet Speed	Jet-Substrate Distance	Ionization Gas Flow Rate	Carrier Gas Flow Rate	Number of Deposition Passes
PT3	3 g/h	500 W	50%	1 m/min	30 mm	500 L/h	400 L/h	1
PT3x3	3 g/h	500 W	50%	1 m/min	30 mm	500 L/h	400 L/h	3
PT5	5 g/h	500 W	50%	1 m/min	30 mm	500 L/h	400 L/h	1
PT5x3	5 g/h	500 W	50%	1 m/min	30 mm	500 L/h	400 L/h	3
PT5x6	5 g/h	500 W	50%	1 m/min	30 mm	500 L/h	400 L/h	6

A JSM-7600F scanning electron microscope (SEM) manufactured by JEOL® (Tokyo, Japan) was used to acquire images of coating's surface structure before and after icing/de-icing. Presence of various chemical functions on the surface was studied through Fourier transform infrared spectroscopy (FTIR). A Bruker Vertex 70 FTIR system (Billerica, MA, USA) was used in ATR mode with a resolution of 2 cm^{-1}. Each of the FTIR spectra presented in this paper were averaged over 32 consecutive scans on the sample, and the data acquisition and analysis was done using the Bruker-provided software, called OPUS (version 8.2). Further chemical analysis on the chemical composition of the surface and the chemical state of silicon was performed using an X-ray photoelectron spectrometer (XPS) with a non-monochromatic Al (max energy 1486.6 eV) anode manufactured by Staib Instruments® (Langenbach, Germany). Scanning parameters used for the acquisition of survey and high-resolution spectra are presented in Table 2. All analyses on the spectra were performed using CasaXPS software (version 2.3.22). Charge compensation was performed by fitting a synthetic peak in C 1*s* envelope and then calibrating the peak position to 284.5 eV.

Table 2. Acquisition parameters for survey and high resolution X-ray photoelectron spectrometer (XPS) spectra.

	Start Energy	End Energy	Step Width	dE	Dwell Time	# of Scans	Beam Power
Survey	1300 eV	0 eV	1 eV	4 eV	100 ms	5	150 W
High resolution	A ~ 20eV window around the peak		0.1 eV	0.3 eV	300 ms	10	300 W

All water contact angle measurements were performed using a DSA100 goniometer manufactured by Kruss® (Hamburg, Germany). Static contact angle was measured by placing a 4 µL droplet on the surface and calculating the angle at the three-phase interface based on Young–Laplace approximation. Static contact angle values presented here are the average of at least 15 measurements on different locations and/or samples. To evaluate the dynamic wetting behavior, at first the needle was placed close to the surface and a 4 µL droplet was deposited on the surface. Then the volume of this droplet was steadily increased to 13 µL with a rate of 3 µL/min. The contact angle on each side of the droplet was measured five times per second using the tangent method. Advancing contact angle can then be defined based on the contact angle vs. time curve. Similarly, the receding contact angle was defined by reducing the droplet volume back to its initial value and constantly measuring the contact angle of the moving interfaces. For more information on this procedure, see [62,63].

The same goniometer along with a Photron SA1.1 (675K-M2) high-speed camera (Photron, Tokyo, Japan) was used to study the droplet mobility on the coatings. This camera is capable of recording videos with up to 60,000 frames per second, but for droplet mobility studies the frame rate was set to 5400 fps to maintain a sufficient image resolution. Initially, a 10 µL droplet was generated in the goniometer. This large droplet size was chosen in order to highlight the shape distortion and droplet

disintegration during rebound. This droplet was then forced to free-fall towards the coating from a 300-mm height and the bouncing behavior was recorded with the high-speed camera.

A horizontal wind tunnel with a total air flow path of 30 m operating in sub-zero temperatures was used to simulate natural atmospheric icing conditions. The schematics of this wind tunnel are presented in Figure 3. It was equipped with three water nozzles which were responsible for the generation of a super-cooled mist from which the ice grows. Prior to icing, samples were kept at −10 °C for at least 1 h. The samples were then mounted on aluminum beams and were placed vertically in the test section of the wind tunnel, facing the nozzles. The operational conditions of the wind tunnel are presented in Table 3.

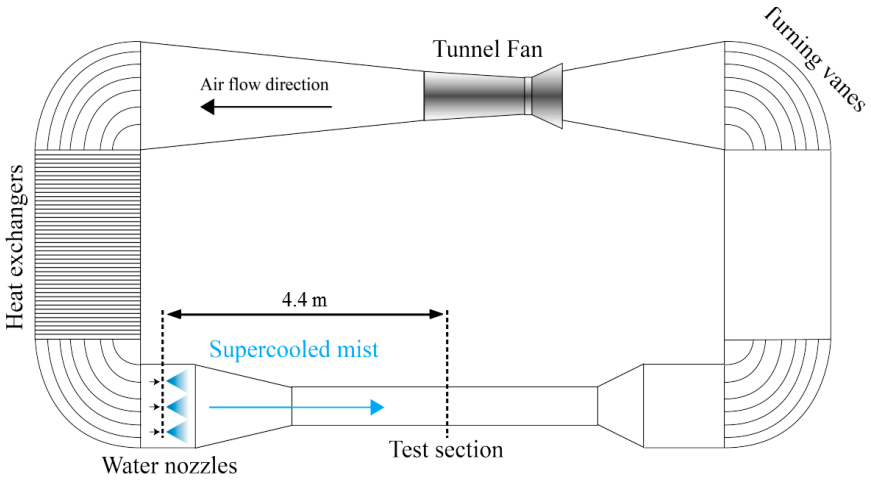

Figure 3. Schematics of the wind tunnel used for ice accumulation.

Table 3. Icing conditions used in the wind tunnel for ice accumulation.

Wind Velocity at the Test Section	Air Temperature	Water Pressure	Air Pressure	Droplet Mean Volume Diameter	Liquid Water Content
10 m/s	−10 °C	325 kPa	100 kPa	63.3 μm	1.8 gr/m^3

The samples were exposed to the conditions presented in Table 3 for 9 min (which correlates to an ice thickness of roughly 1 cm) before being returned into a cold room at −10 °C. Iced surfaces were then kept at −10 °C for 20 min before the de-icing procedure using a homemade centrifugal instrument. De-icing was performed by rotating the beams at a controlled speed and measuring the rotational speed at which the ice detaches from the surface. The ice adhesion strength can then be determined according to:

$$\tau = mr\omega^2/A \quad (2)$$

where τ is the ice adhesion strength (kPa), m is the mass of the accumulated ice (kg), r is the beam radius (0.17 m), ω is the rotational speed of the beam at the point of ice detachment (rpm), and A is the contact area between the ice and the surface (m^2).

3. Results and Discussion

A comprehensive characterization of these coatings prior to any icing/de-icing cycles has already been published [60,64]. Through FTIR and XPS studies, it was shown that the surface structure consists of a Si–O network backbone with organic functions replacing oxygen atoms at some positions. Furthermore, SEM analysis showed a hierarchical structure with features ranging from tens of micrometers to only a few nanometers. This nanometric surface structure, along with the inclusion of low-surface-energy organic groups in the silica network, results in a superhydrophobic surface with static contact angles higher than 150° and contact angle hysteresis lower than 6°. In this paper,

the icephobic behavior of superhydrophobic coatings are emphasized and the effects of multiple icing/de-icing cycles on surface properties is studied.

3.1. Wetting Behavior and Icephobic Properties

All surface developed here are superhydrophobic with nearly perfect roll-off behavior. Static contact angles and contact angle hysteresis for these surfaces prior to icing are presented in Figure 4.

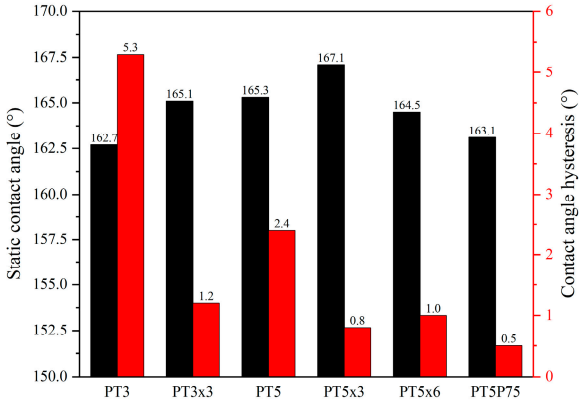

Figure 4. Static contact angle and contact angle hysteresis before icing/de-icing cycles.

As mentioned before, droplet mobility, for which contact angle hysteresis may act as a representation, plays an important role in prevention of ice accumulation or reducing the ice adhesion strength. A water droplet striking a superhydrophobic surface will expand to a maximum diameter (splash disk) and then recoils, bouncing off the surface [65]. Ice accumulation may be reduced or prevented if the time required for the nucleation and growth of ice crystals is longer than the time during which the droplet is in contact with the surface [44]. Here, through high-speed imaging of the interaction between a free-falling water droplet and the developed coatings, droplet mobility on the surface is demonstrated. Furthermore, based on the number of frames in which the droplet is in contact with the water, it is possible to determine the contact duration. In Figure 5, a few frames from the video acquired for PT5x3 are presented as an example.

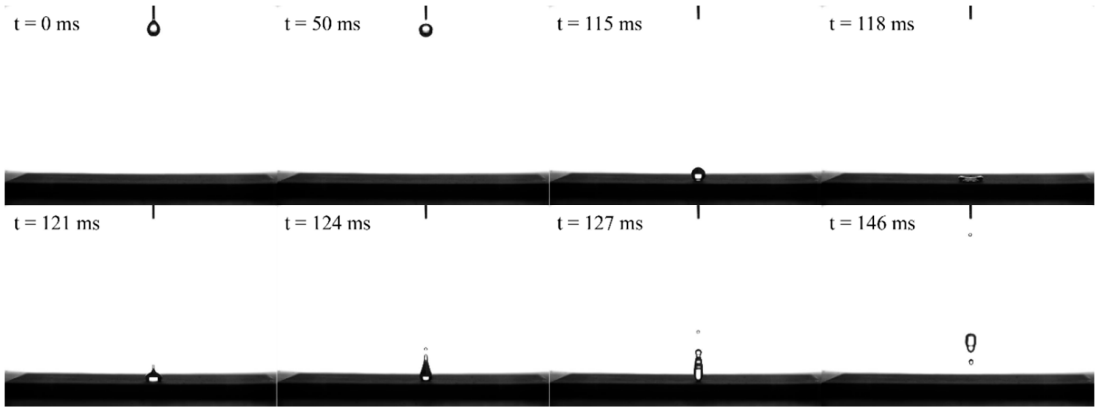

Figure 5. Selected frames from the high-speed video acquired from a 10 μL droplet (13 mm diameter) free-falling from a 300-mm height on PT5x3.

The impact times (derived from the full videos) for all plasma-deposited coatings are presented in Figure 6. It is shown that the impact time for all the coatings studied here is less than 15 ms. The time required for a droplet to freeze on a surface is heavily affected by the droplet temperature, speed, and size, along with surface temperature, morphology, and thermal conductivity. However, it has

been shown that on a completely wetted surface (hydrophilic surface), freezing time is in the range of a few seconds [44]. Therefore, the impact time on the superhydrophobic surfaces introduced here are multiple orders of magnitude shorter than the time required for ice crystals to form. This may result in lower ice accumulation all together or may reduce ice adhesion strength by inclusion of air bubbles at the interface.

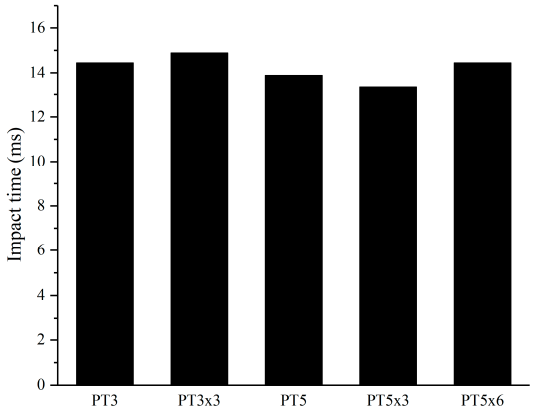

Figure 6. The impact time for a 10 µL droplet for all coatings. Free-fall height is set to 300 mm.

All plasma-deposited coatings presented before are studied regarding their icephobic behavior for three cycles of icing/de-icing. The results are shown in Figure 7.

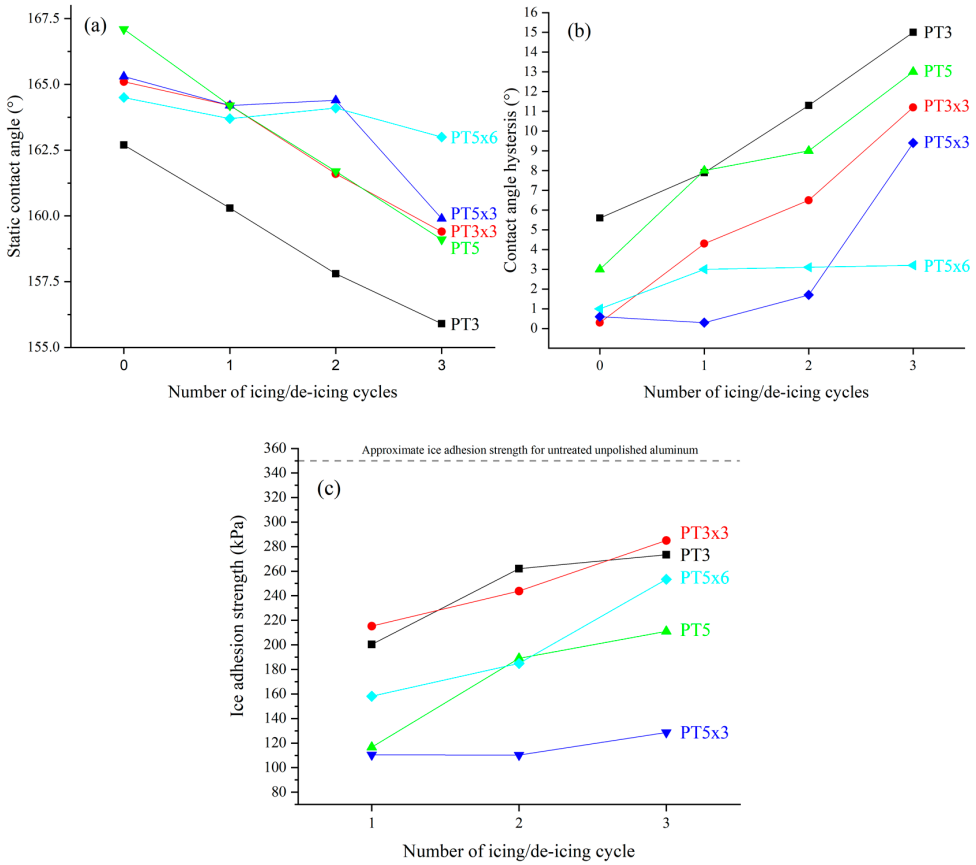

Figure 7. (**a**) Static contact angle, (**b**) contact angle hysteresis, and (**c**) ice adhesion strength for the first three icing/de-icing cycles for PT3, PT3x3, PT5, PT5x3, and PT5x6.

Figure 7a shows the static contact angle and Figure 7b shows the contact angle hysteresis measured after each icing/de-icing cycle while Figure 7c shows the ice adhesion strength for three icing/de-icing cycles. The data presented in Figure 7 are acquired from six separate measurements for each sample. However, due to the inherently chaotic nature of ice fracture, some measurements were deemed inconclusive. For instance, samples that exhibit cohesive failure (failure in the ice bulk instead of the ice/substrate interface) or partial removal of ice were not considered in the average values presented here. Error bars are omitted from Figure 7 to improve clarity and highlight the observed data trends, but are retained in Figure 8 for the most efficient coating (PT5x3).

In most cases, static contact angle decreases with the number of icing/de-icing cycles. This decreasing trend is more pronounced for single pass coatings (PT3 and PT5) compared to multi-pass coatings (PT3x3, PT5x3, and PT5x6), which suggests a partial removal of the coating during de-icing. After the first cycle, there is a small decrease in the static contact angle on PT3x3, PT5x3, and PT5x6. However, after the second cycle, static contact angle for PT3x3 decreases more significantly, but no remarkable decrease in the contact angle for PT5x3 and PT5x6 is observed. Finally, after the third cycle, there is a rather large drop in the static contact angle for PT5x3, but this decrease is not observed in PT5x6. Since one would expect PT5x3 to be thicker than PT3x3 and thinner than PT5x6, this trend confirms the correlation between coating thickness and the effects of de-icing on wetting behavior. In other words, PT5x6 is thicker than PT5x3 and PT3x3, and therefore it can retain its hydrophobicity even after significant coating removal. This is also demonstrated in the increasing trend in contact angle hysteresis with the number of icing/deicing cycles: single pass coatings exhibit the largest increase in the contact angle hysteresis, and this increase becomes smaller and smaller as the coating thickness increases. This was also confirmed by Wang et al., where a direct correlation was found between coating thickness and ice adhesion strength [66].

While studying icing behavior, it should be noted that ice adhesion strength cannot be directly correlated to wetting behavior or to contact angle: a hydrophobic or a superhydrophobic surface may be considered as a good candidate for icephobic properties, but to confirm icephobic behavior, ice adhesion needs to be studied separately. For instance, a coating may exhibit superhydrophobic behavior when a water droplet is placed on the surface without any excessive force (as is the case in most goniometry studies), but atmospheric ice is generally formed due to the impinging supercooled droplets, and thus the effects of kinetic energy transfer, droplet splashing, and droplet disintegration cannot be ignored (see Figure 5).

For all icing/de-icing cycles, the samples prepared with a precursor flow rate of 3 g/h (PT3 and PT3x3) exhibit higher ice adhesion strength compared to those prepared with a precursor flow rate of 5 g/h (PT5, PT5x3, and PT5x6). This seems to be due to the higher coating thickness and higher presence of hydrophobic groups on the surface [60,64]. Furthermore, PT3 and PT3x3 exhibit similar icephobic behavior, but this similarity is not observed in the case of PT5, PT5x3, and PT5x6. In these cases, the effects of coating removal after each de-icing is more apparent. PT5 and PT5x3 exhibit almost identical ice adhesion strengths for the first icing cycle, attesting to similar surface structure and icing behavior. However, ice adhesion strength rapidly increases with the number of icing/de-icing cycles for PT5, whereas this increase is not observed for PT5x3. This may correspond to a partial coating removal from both surfaces, which in the case of PT5 will lead to the underlying porous structure being exposed to the icing medium thus increases the ice adhesion strength. Since the coating is thicker in the case of PT5x3, coating removal after the first cycle is not as influential, and the icephobic surface structure may be retained on the surface. For PT5x6, ice adhesion strength increases significantly with the number of icing/de-icing cycles, which can be explained by the morphological differences between PT5x3 and PT5x6: recently, we have found that the agglomeration of deposited particles during six passes of plasma deposition in the atmospheric pressure plasma jet leads to the deposition of significantly larger silica-based particulates on the substrate [60,64]. These larger particulates become mechanically unstable, resulting in the appearance of a white powder on the substrate, which is easily

removed. These particulates may be heavily affected by the impinging water droplets or by the wind speed, resulting in a lower mechanical stability of the surface structure.

Based on the results acquired for the first three icing/de-icing cycles, PT5x3 was identified as the most promising coating for further studies. In this context, icing/de-icing cycles were continued on PT5x3 for 10 consecutive cycles. Figure 8 shows the ice adhesion strength along with advancing and receding contact angles on PT5x3 for 10 cycles of icing/de-icing. The increasing trend in ice adhesion strength confirms the removal of the coating materials during de-icing. It can be observed that for the first nine icing/de-icing cycles, ice adhesion strength on PT5x3 is reduced by a factor of at least two compared to the ice adhesion strength on unpolished aluminum substrates. Ice adhesion strength increases to 228 kPa for the 10th cycle, which is more than double the ice adhesion strength for the first cycle.

From Figure 8, it is clear that ice adhesion strength follows a similar trend to that of receding contact angle: the in the receding angle after the second cycle corresponds to an increase in ice adhesion strength. Ice adhesion strength then remains constant for the next three cycles, during which receding angle is constant. Finally, ice adhesion strength increases after the seventh icing/de-icing cycle, where receding angle also decreases. A similar correlation between ice adhesion strength and receding angle was also suggested by Meuler et al. [6] for a flat surface. Plotting the data acquired in this study against the data presented in [6] (which is in turn deduced from their own measurements along with two other icing-related studies, [4,29]) suggests that a similar linear correlation exists between the ice adhesion strength of the developed organosilicon based coatings with ice adhesion strength (see Figure 9). It should be noted that this correlation is shown to be independent, at least to some degree, of the ice adhesion measurement method and icing conditions.

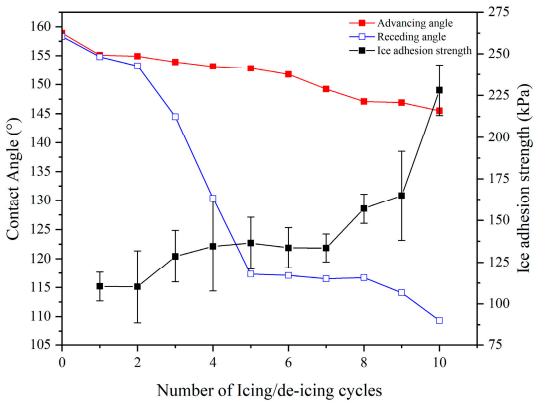

Figure 8. Ice adhesion strength and contact angles on PT5x3 for up to 10 cycles of icing/de-icing.

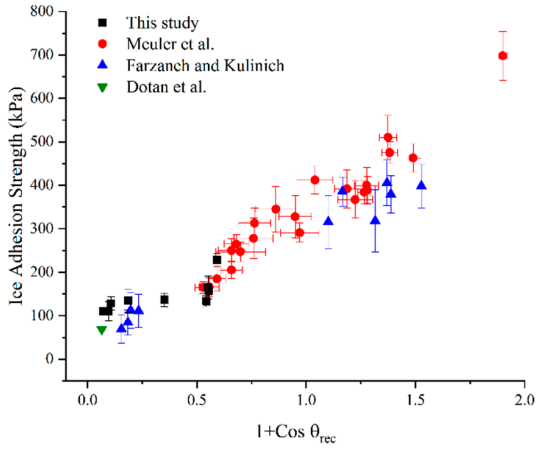

Figure 9. Correlation between ice adhesion strength and the practical work of adhesion (see Equation (1)) compared with the data derived from [4,6,29].

3.2. Surface Morphology

Surface morphology of the deposited coatings before and after multiple icing/deicing cycles was studied using scanning electron microscopy and the results are presented in Figure 10. More detailed and comprehensive analyses of coatings' surface structure before icing were recently published by the authors [60,64]. Therefore, in this paper, the effects of icing/deicing cycles and aggressive environments on coatings surface structure is emphasized. It should be noted that as will be discussed later, PT5x3 exhibited the best icephobic behavior among the coatings being discussed here. Subsequently, to better evaluate its stability, 10 cycles of icing/deicing were performed for PT5x3. For the rest of the coatings, only three cycles were carried out.

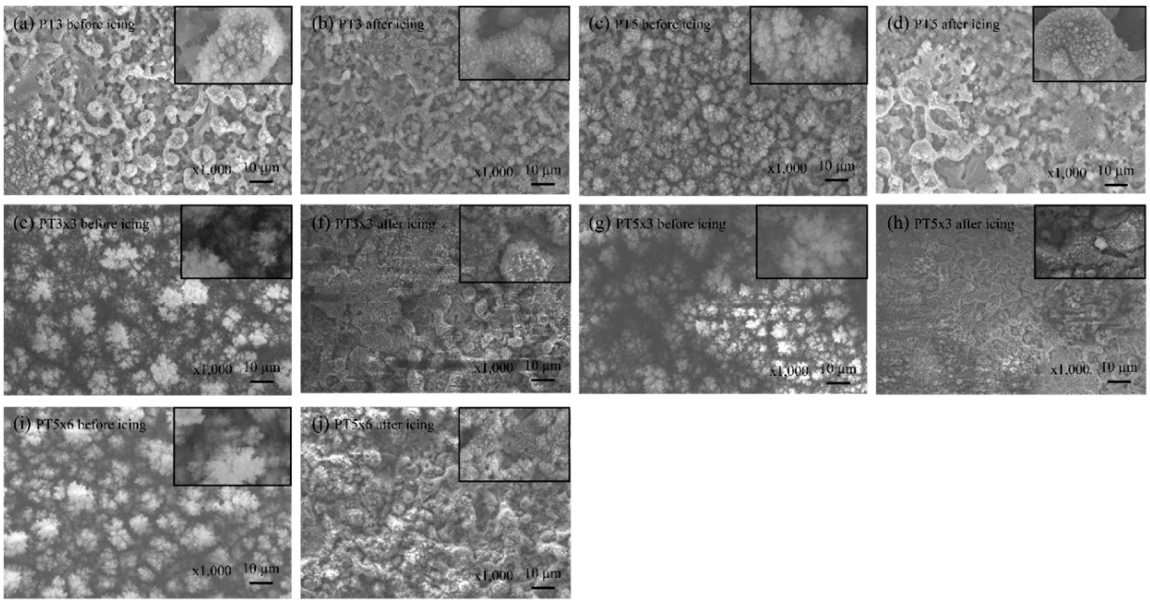

Figure 10. Scanning electron microscope (SEM) images of the plasma-deposited coatings before and after icing/deicing cycles (insets are taken with ×10,000 magnification to better show the surface structure): (**a**) PT3 before icing, (**b**) PT3 after icing, (**c**) PT5 before icing, (**d**) PT5 after icing, (**e**) PT3x3 before icing, (**f**) PT3x3 after icing, (**g**) PT5x3 before icing, (**h**) PT5x3 after icing, (**i**) PT5x6 before icing, (**j**) PT5x6 after icing. For PT5x3, SEM images were acquired after 10 cycles of icing/de-icing, whereas for the rest of the samples they were acquired after 3 cycles of icing/de-icing.

From Figure 10, it is clear that a certain degree of coating removal is observed on all coatings after multiple icing/de-icing cycles. This is most likely due to the aggressive de-icing method used in this study, which may remove a part of the surface structure along with the accumulated ice. Sufficient coating removal may expose the underlying micro porous substrate to the icing medium, leading to a larger ice/substrate interfacial area and increasing the ice adhesion strength compared to the untreated sample. Note that in nature, ice removal is typically not as aggressive, and therefore 10 cycles of icing/de-icing as discussed in this paper cannot be correlated to 10 icing events in practical applications.

3.3. Surface Chemistry

Chemical composition of the coatings being discussed here was extensively studied in previous publications [60,64]. Through FTIR spectroscopy and high resolution XPS analysis of Si 2*p* core peak, it was suggested that the backbone of the surface structure (before icing) is a Si–O–Si matrix with hydrophobic organic groups replacing oxygen atoms at some positions. In this paper, the effects of icing/de-icing cycles on surface chemistry is emphasized. The results are shown in Figure 11.

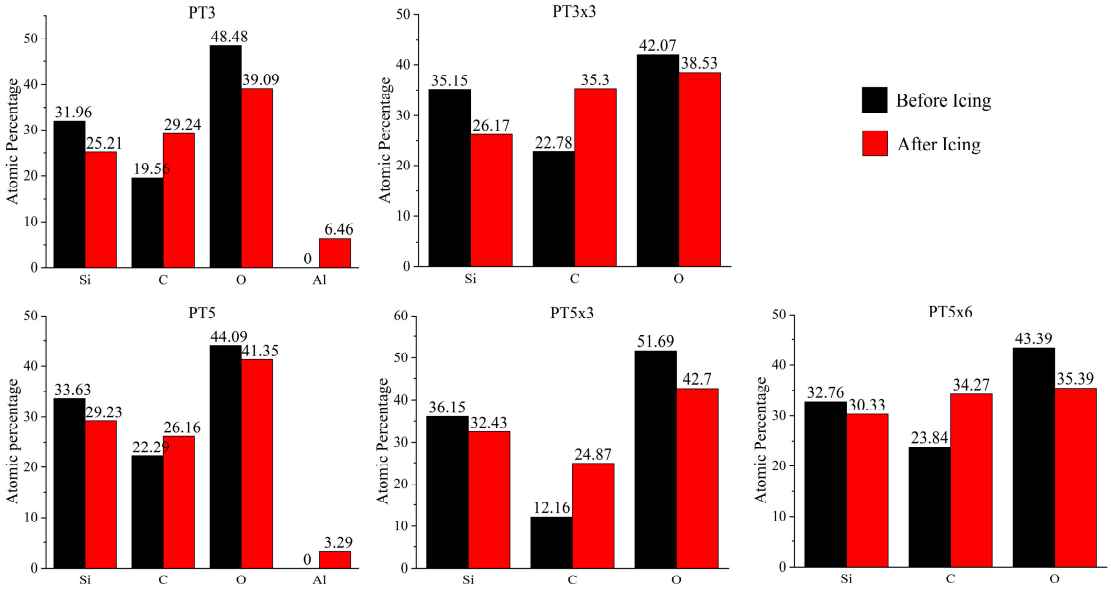

Figure 11. Atomic percentages of silicon, carbon, aluminum and oxygen on all coatings derived from XPS.

In all cases, multiple cycles of icing/de-icing leads to a reduction in the atomic percentage of oxygen and silicon while increasing the atomic percentage of carbon. This corresponds to the removal of Si–O–Si structures from the surface due to the aggressive de-icing procedure used in this study. In fact, in PT3 and PT5, where coating thickness is expected to be lower than other cases, Al peak is observed in the XPS spectra acquired from the surfaces after three passes of icing/deicing: during de-icing, silicon-based structure is partially removed from the surface, exposing the underlying alumina-based structure. In other cases, since the coating is thicker, substrate is not exposed to the X-ray emission and therefore no Al peak is observed.

4. Conclusions

An environmentally friendly and economically feasible approach to the development of organosilicon-based superhydrophobic/icephobic coatings on Al-6061 substrates was reported. Multiple samples were developed with varying precursor flow rate and number of deposition passes. To estimate the coatings' efficiency against aggressive natural conditions, ice adhesion strength was measured on all samples for three cycles of icing/de-icing. Coating removal during aggressive de-icing procedure was demonstrated on all samples. All samples were shown to reduce ice adhesion strength to some degree, with PT5x3 showing the best icephobic efficiency over the range of experimental conditions studied. This coating was capable of reducing the ice adhesion strength by a factor of 2 for at least nine cycles of icing de-icing. A correlation was found between ice adhesion strength and receding contact angle, although the exact nature of this correlation remains unknown. Due to the versatility of the main reactor used in this study (an atmospheric pressure plasma jet open to ambient air), the procedure introduced here may be easily implemented in large-scale industrial applications, such as in-line production of icephobic high voltage cables. Further improvement in the coating's efficiency in icing conditions may be possible through fine-tuning of some of the plasma parameters studied here and considering some other parameters that were not considered in the present work, such as jet-substrate distance or the plasma gas and its flow rate. In this context, the cost to efficiency ratio should be considered. For instance, using argon or helium instead of nitrogen as the plasma gas may improve the icephobic behavior of the coating by reducing the amount of high surface energy nitrogen-based species on the surface, but these gases are more expensive than nitrogen, and thus the process cost

would increase significantly. Furthermore, the mechanical stability of the coating may be improved through some plasma or non-plasma based post-treatment procedures.

Author Contributions: Conceptualization, S.A., M.F., and L.S.; methodology, S.A.; validation, S.A.; formal analysis, S.A.; investigation, S.A.; data curation, S.A.; writing—original draft preparation, S.A.; writing—review and editing, S.A., M.F. and L.S.; supervision, M.F. and L.S.; project administration, M.F. and L.S.; funding acquisition, M.F. and L.S.

Funding: This research was funded by the NSERC/Hydro-Québec/UQAC Industrial Chair on Atmospheric Icing of Power Network Equipment (CIGELE), the Canada Research Chair on Engineering of Power Network Atmospheric Icing (INGIVRE) at Université du Québec a Chicoutimi, the Chaire de Recherche du Canada en Physique des Plasmas HAutement RÉactifs (PPHARE) at Université de Montréal, and the NSERC's Green-SEAM (Surface Engineering And Manufacturing) network.

Acknowledgments: The authors would like to thank Andranik Sarkissian of Plasmionique for his valuable comments and guidance throughout this study.

Conflicts of Interest: The authors declare no conflict of interest.

References

1. *The 1998 Ice Storm: 10-Year Retrospective—RMS Special Report*; Risk Management Solutions, Inc.: New Ark, CA, USA, 2008.
2. Farzaneh, M. Atmospheric icing of power networks. In *Atmospheric Icing of Power Networks*; Springer: Berlin, Germany, 2008; pp. 1–381.
3. Eliasson, A.J.; Farzaneh, M.; Fikke, S.M.; Haldar, A.; Isozaki, M.; Jakl, F.; Lake, R.; Leblond, A.; Minchin, M.; Mito, M.; et al. *CIGRE Working Group B2.29: Systems for Prediction and Monitoring of Ice Shedding, Anti-Icing and De-Icing for Power Line Conductors and Ground Wires*; University of Huddersfield: Huddersfield, UK, 2010.
4. Kulinich, S.A.; Farzaneh, M. How wetting hysteresis influences ice adhesion strength on superhydrophobic surfaces. *Langmuir* **2009**, *25*, 8854–8856. [CrossRef] [PubMed]
5. Farhadi, S.; Farzaneh, M.; Kulinich, S.A. Anti-icing performance of superhydrophobic surfaces. *Appl. Surf. Sci.* **2011**, *257*, 6264–6269. [CrossRef]
6. Meuler, A.J.; Smith, J.D.; Varanasi, K.K.; Mabry, J.M.; McKinley, G.H.; Cohen, R.E. Relationships between water wettability and ice adhesion. *ACS Appl. Mater. Interfaces* **2010**, *2*, 3100–3110. [CrossRef] [PubMed]
7. Subramanyam, S.B.; Rykaczewski, K.; Varanasi, K.K. Ice adhesion on lubricant-impregnated textured surfaces. *Langmuir* **2013**, *29*, 13414–13418. [CrossRef] [PubMed]
8. Varanasi, K.K.; Deng, T.; Smith, J.D.; Hsu, M.; Bhate, N. Frost formation and ice adhesion on superhydrophobic surfaces. *Appl. Phys. Lett.* **2010**, *97*, 234102. [CrossRef]
9. Makkonen, L. Ice adhesion—Theory, measurements and countermeasures. *J. Adhes. Sci. Technol.* **2012**, *26*, 413–445.
10. Srikanth, N.; Liu, E.; Wilson, P.; Chen, Z. Development of sol–gel icephobic coatings: Effect of surface roughness and surface energy. *Appl. Mater. Interfaces* **2014**, *6*, 20685–20692.
11. Sarkar, D.K.; Farzaneh, M. Superhydrophobic coatings with reduced ice adhesion. *J. Adhes. Sci. Technol.* **2009**, *23*, 1215–1237. [CrossRef]
12. Wang, Y.; Xue, J.; Wang, Q.; Chen, Q.; Ding, J. Verification of icephobic/anti-icing properties of a superhydrophobic surface. *ACS Appl. Mater. Interfaces* **2013**, *5*, 3370–3381. [CrossRef]
13. Tourkine, P.; Merrer, M.L.; Quéré, D. Delayed freezing on water repellent materials. *Langmuir* **2009**, *25*, 7214–7216. [CrossRef]
14. Cao, L.; Jones, A.K.; Sikka, V.K.; Wu, J.; Gao, D. Anti-icing superhydrophobic coatings. *Langmuir* **2009**, *25*, 12444–12448. [CrossRef]
15. Zhu, L.; Xue, J.; Wang, Y.; Chen, Q.; Ding, J.; Wang, Q. Ice-phobic coatings based on silicon-oil-infused polydimethylsiloxane. *ACS Appl. Mater. Interfaces* **2013**, *5*, 4053–4062. [CrossRef] [PubMed]
16. Laforte, C.; Laforte, J.L. Deicing strains and stresses of iced substrates. *J. Adhes. Sci. Technol.* **2012**, *26*, 603–620.
17. Susoff, M.; Siegmann, K.; Pfaffenroth, C.; Hirayama, M. Evaluation of icephobic coatings—Screening of different coatings and influence of roughness. *Appl. Surf. Sci.* **2013**, *282*, 870–879. [CrossRef]

18. Tarquini, S.; Antonini, C.; Amirfazli, A.; Marengo, M.; Palacios, J. Investigation of ice shedding properties of superhydrophobic coatings on helicopter blades. *Cold Reg. Sci. Technol.* **2014**, *100*, 50–58. [CrossRef]
19. Kulinich, S.A.; Farzaneh, M. Ice adhesion on super-hydrophobic surfaces. *Appl. Surf. Sci.* **2009**, *255*, 8153–8157. [CrossRef]
20. Shirtcliffe, N.J.; McHale, G.; Newton, M.I. The superhydrophobicity of polymer surfaces: Recent developments. *J. Polym. Sci. Part B Polym. Phys.* **2011**, *49*, 1203–1217. [CrossRef]
21. Farzaneh, M.; Sarkar, D.K. Nanostructured superhydrophobic coatings. *J. CPRI* **2008**, *4*, 135–147.
22. Alizadeh, A.; Yamada, M.; Li, R.; Shang, W.; Otta, S.; Zhong, S.; Ge, L.; Dhinojwala, A.; Conway, K.R.; Bahadur, V.; et al. Dynamics of ice nucleation on water repellent surfaces. *Langmuir* **2012**, *28*, 3180–3186. [CrossRef]
23. Jafari, R.; Menini, R.; Farzaneh, M. Superhydrophobic and icephobic surfaces prepared by RF-sputtered polytetrafluoroethylene coatings. *Appl. Surf. Sci.* **2010**, *257*, 1540–1543. [CrossRef]
24. Mobarakeh, L.F.; Jafari, R.; Farzaneh, M. Superhydrophobic surface elaboration using plasma polymerization of hexamethyldisiloxane (HMDSO). *Adv. Mater. Res.* **2011**, *409*, 783–787. [CrossRef]
25. Dodiuk, H.; Kenig, S.; Dotan, A. Do self-cleaning surfaces repel ice? *J. Adhes. Sci. Technol.* **2012**, *26*, 701–714.
26. Wang, H.; He, G.; Tian, Q. Effects of nano-fluorocarbon coating on icing. *Appl. Surf. Sci.* **2012**, *258*, 7219–7224. [CrossRef]
27. Mittal, K.L. Adhesion measurement of thin films. *Act. Passiv. Electron. Compon.* **1976**, *3*, 21–42. [CrossRef]
28. Gao, L.; McCarthy, T.J. Wetting 101? *Langmuir* **2009**, *25*, 14105–14115. [CrossRef]
29. Dotan, A.; Dodiuk, H.; Laforte, C.; Kenig, S. The relationship between water wetting and ice adhesion. *J. Adhes. Sci. Technol.* **2009**, *23*, 1907–1915. [CrossRef]
30. Meuler, A.J.; McKinley, G.H.; Cohen, R.E. Exploiting topographical texture to impart icephobicity. *ACS Nano* **2010**, *4*, 7048–7052. [CrossRef]
31. Chen, J.; Liu, J.; He, M.; Li, K.; Cui, D.; Zhang, Q.; Zeng, X.; Zhang, Y.; Wang, J.; Song, Y. Superhydrophobic surfaces cannot reduce ice adhesion. *Appl. Phys. Lett.* **2012**, *101*, 111603. [CrossRef]
32. Nosonovsky, M.; Hejazi, V. Why superhydrophobic surfaces are not always icephobic. *ACS Nano* **2012**, *6*, 8488–8491. [CrossRef]
33. Oberli, L.; Caruso, D.; Hall, C.; Fabretto, M.; Murphy, P.J.; Evans, D. Condensation and freezing of droplets on superhydrophobic surfaces. *Adv. Colloid Interface Sci.* **2014**, *210*, 47–57. [CrossRef]
34. Bahadur, V.; Mishchenko, L.; Hatton, B.; Taylor, J.A.; Aizenberg, J.; Krupenkin, T. Predictive model for ice formation on superhydrophobic surfaces. *Langmuir* **2011**, *27*, 14143–14150. [CrossRef] [PubMed]
35. Guo, P.; Zheng, Y.; Wen, M.; Song, C.; Lin, Y.; Jiang, L. Icephobic/anti-icing properties of micro/nanostructured surfaces. *Adv. Mater.* **2012**, *24*, 2642–2648. [CrossRef] [PubMed]
36. Wang, F.; Li, C.; Lv, Y.; Lv, F.; Du, Y. Ice accretion on superhydrophobic aluminum surfaces under low-temperature conditions. *Cold Reg. Sci. Technol.* **2010**, *62*, 29–33. [CrossRef]
37. Antonini, C.; Innocenti, M.; Horn, T.; Marengo, M.; Amirfazli, A. Understanding the effect of superhydrophobic coatings on energy reduction in anti-icing systems. *Cold Reg. Sci. Technol.* **2011**, *67*, 58–67. [CrossRef]
38. Zhang, Y.; Yu, X.; Wu, H.; Wu, J. Facile fabrication of superhydrophobic nanostructures on aluminum foils with controlled-condensation and delayed-icing effects. *Appl. Surf. Sci.* **2012**, *258*, 8253–8257. [CrossRef]
39. Li, P.; Li, L.; Wang, W.; Jin, W.; Liu, X.; Yeung, K.W.K.; Chu, P.K. Enhanced corrosion resistance and hemocompatibility of biomedical NiTi alloy by atmospheric-pressure plasma polymerized fluorine-rich coating. *Appl. Surf. Sci.* **2014**, *297*, 109–115. [CrossRef]
40. Sarshar, M.A.; Swarctz, C.; Hunter, S.; Simpson, J.; Choi, C.H. Effects of contact angle hysteresis on ice adhesion and growth on superhydrophobic surfaces under dynamic flow conditions. *Colloid Polym. Sci.* **2013**, *291*, 427–435. [CrossRef]
41. Kulinich, S.A.; Farhadi, S.; Nose, K.; Du, X.W. Superhydrophobic surfaces: Are they really ice-repellent? *Langmuir* **2011**, *27*, 25–29. [CrossRef]
42. Sojoudi, H.; Wang, M.; Boscher, N.D.; McKinley, G.H.; Gleason, K.K. Durable and scalable icephobic surfaces: Similarities and distinctions from superhydrophobic surfaces. *Soft Matter* **2016**, *12*, 1938–1963. [CrossRef]
43. Fillion, R.M.; Riahi, A.R.; Edrisy, A. A review of icing prevention in photovoltaic devices by surface engineering. *Renew. Sustain. Energy Rev.* **2014**, *32*, 797–809. [CrossRef]

44. Mishchenko, L.; Hatton, B.; Bahadur, V.; Taylor, J.A.; Krupenkin, T.; Aizenberg, J. Design of ice-free nanostructured surfaces based on repulsion of impacting water droplets. *ACS Nano* **2010**, *4*, 7699–7707. [CrossRef] [PubMed]
45. del Cerro, D.A.; Römer, G.R.B.E.; Huis, A.J. Erosion resistant anti-ice surfaces generated by ultra short laser pulses. *Phys. Procedia* **2010**, *5*, 231–235. [CrossRef]
46. Jung, S.; Dorrestijn, M.; Raps, D.; Das, A.; Megaridis, C.M.; Poulikakos, D. Are superhydrophobic surfaces best for icephobicity? *Langmuir* **2011**, *27*, 3059–3066. [CrossRef] [PubMed]
47. Schutzius, T.M.; Jung, S.; Maitra, T.; Eberle, P.; Antonini, C.; Stamatopoulos, C.; Poulikakos, D. Physics of icing and rational design of surfaces with extraordinary icephobicity. *Langmuir* **2015**, *31*, 4807–4821. [CrossRef]
48. Kim, P.; Wong, T.S.; Alvarenga, J.; Kreder, M.J.; Adorno-Martinez, W.E.; Aizenberg, J. Liquid-infused nanostructured surfaces with extreme anti-ice and anti-frost performance. *ACS Nano* **2012**, *6*, 6569–6577. [CrossRef]
49. Yang, S.; Xia, Q.; Zhu, L.; Xue, J.; Wang, Q.; Chen, Q.M. Research on the icephobic properties of fluoropolymer-based materials. *Appl. Surf. Sci.* **2011**, *257*, 4956–4962. [CrossRef]
50. Mei, H.; Luo, D.; Guo, P.; Song, C.; Liu, C.; Zheng, Y.; Jiang, L. Multi-level micro-/nanostructures of butterfly wings adapt at low temperature to water repellency. *Soft Matter* **2011**, *7*, 10569. [CrossRef]
51. He, M.; Li, H.; Wang, J.; Song, Y. Superhydrophobic surface at low surface temperature. *Appl. Phys. Lett.* **2011**, *98*, 093118. [CrossRef]
52. Cassie, A.B.D.; Baxter, S. Wettability of porous surfaces. *Trans. Faraday Soc.* **1944**, *40*, 546–551. [CrossRef]
53. Palumbo, F.; di Mundo, R.; Cappelluti, D.; Dagostino, R. Superhydrophobic and Superhydrophilic polycarbonate by tailoring chemistry and nano-texture with plasma processing. *Plasma Process. Polym.* **2011**, *8*, 118–126. [CrossRef]
54. Pulpytel, J.; Kumar, V.; Peng, P.; Micheli, V.; Laidani, N.; Arefi-Khonsari, F. Deposition of organosilicon coatings by a non-equilibrium atmospheric pressure plasma jet: Design, analysis and macroscopic scaling law of the process. *Plasma Process. Polym.* **2011**, *8*, 664–675. [CrossRef]
55. Lommatzsch, U.; Ihde, J. Plasma polymerization of HMDSO with an atmospheric pressure plasma jet for corrosion protection of aluminum and low-adhesion surfaces. *Plasma Process. Polym.* **2009**, *6*, 642–648. [CrossRef]
56. Siliprandi, R.A.; Zanini, S.; Grimoldi, E.; Fumagalli, F.S.; Barni, R.; Riccardi, C. Atmospheric pressure plasma discharge for polysiloxane thin films deposition and comparison with low pressure process. *Plasma Chem. Plasma Process.* **2011**, *31*, 353–372. [CrossRef]
57. Kakiuchi, H.; Higashida, K.; Shibata, T.; Ohmi, H.; Yamada, T.; Yasutake, K. High-rate HMDSO-based coatings in open air using atmospheric-pressure plasma jet. *J. Non Cryst. Solids* **2012**, *358*, 2462–2465. [CrossRef]
58. Hare, E.; Shafrin, E.; Zisman, W. Properties of films of adsorbed fluorinated acids. *J. Phys. Chem.* **1954**, *513*, 236–239. [CrossRef]
59. Mobarakeh, L.F.; Jafari, R.; Farzaneh, M. Robust icephobic, and anticorrosive plasma polymer coating. *Cold Reg. Sci. Technol.* **2018**, *151*, 89–93. [CrossRef]
60. Asadollahi, S.; Profili, J.; Farzaneh, M.; Stafford, L. Development of organosilicon-based superhydrophobic coatings through atmospheric pressure plasma polymerization of HMDSO in nitrogen plasma. *Materials* **2019**, *12*, 219. [CrossRef]
61. Asadollahi, S.; Farzaneh, M.; Stafford, L. Highly porous micro-roughened structures developed on aluminum surface using the jet of rotating arc discharges at atmospheric pressure. *J. Appl. Phys.* **2018**, *123*, 073302. [CrossRef]
62. Kietzig, A.M. Comments on "an essay on contact angle measurements"—An illustration of the respective influence of droplet deposition and measurement parameters. *Plasma Process. Polym.* **2011**, *8*, 1003–1009. [CrossRef]
63. Müller, M.; Oehr, C. Comments on "an essay on contact angle measurements" by Strobel and Lyons. *Plasma Process. Polym.* **2011**, *8*, 19–24. [CrossRef]
64. Asadollahi, S.; Profili, J.; Farzaneh, M.; Stafford, L. Multi-pass deposition of organosilicon-based superhydrophobic coatings in atmospheric pressure plasma deposition of HMDSO. *Plasma Process. Polym.* **2019**, submitted.

65. Bird, J.C.; Dhiman, R.; Kwon, H.M.; Varanasi, K.K. Reducing the contact time of a bouncing drop. *Nature* **2013**, *503*, 385–388. [CrossRef] [PubMed]
66. Wang, C.; Fuller, T.; Zhang, W.; Wynne, K.J. Thickness dependence of ice removal stress for a polydimethylsiloxane nanocomposite: Sylgard 184. *Langmuir* **2014**, *30*, 12819–12826. [CrossRef] [PubMed]